Novel Mechanistic Insights into Arginine Deiminase Pharmacology Suggest ^{18}F-FDG Is Not Suitable to Evaluate Clinical Response in Melanoma

Lars Stelter[1,2], Michael J. Evans[3], Achim A. Jungbluth[4], Pat Zanzonico[1], Gerd Ritter[4], Thomas Ku[1], Eric Rosenfeld[1], John S. Bomalaski[5], Lloyd Old[4], and Steven M. Larson[1,4,6]

[1]Nuclear Medicine Service, Department of Radiology, Memorial Sloan-Kettering Cancer Center, New York, New York; [2]Department of Radiology and Nuclear Medicine, Charité CVK, Universtätsmedizin Berlin, Berlin, Germany; [3]Human Oncology and Pathogenesis Program, Memorial Sloan-Kettering Cancer Center, New York, New York; [4]Ludwig Institute for Cancer Research, Memorial Sloan-Kettering Cancer Center, New York, New York; [5]Polaris Group, San Diego, California; and [6]Program in Molecular Pharmacology and Chemistry, Memorial Sloan-Kettering Cancer Center, New York, New York

Because of deficiencies in L-arginine biosynthesis, some cancers are susceptible to therapeutic intervention with arginine deiminase (ADI), an enzyme responsible for consuming the dietary supply of L-arginine to deprive the disease of an essential nutrient. ADI is currently being evaluated in several clinical trials, and fully realizing the drug's potential will depend on invoking the appropriate metrics to judge clinical response. Without a clear biologic mandate, PET/CT with ^{18}F-FDG is currently used to monitor patients treated with ADI. However, it is unclear if it can be expected that ^{18}F-FDG responses will indicate (or predict) clinical benefit. **Methods:** ^{18}F-FDG responses to ADI therapy were studied in preclinical models of melanoma in vitro and in vivo. The molecular mechanism of response to ADI therapy was also studied, with a particular emphasis on biologic pathways known to regulate ^{18}F-FDG avidity. **Results:** Although proliferation of SK-MEL 28 was potently inhibited by ADI treatment in vitro and in vivo, no clear declines in ^{18}F-FDG uptake were observed. Further investigation showed that ADI treatment induces the posttranslational degradation of phosphatase and tensin homolog and the activation of the PI3K signaling pathway, an event known to enhance glycolysis and ^{18}F-FDG avidity. A more thorough mechanistic study showed that ADI triggered a complex mechanism of cell death, involving apoptosis via poly (ADP-ribose) polymerase cleavage—independent of caspase 3. **Conclusion:** These findings suggest that some unexpected pharmacologic properties of ADI preclude using ^{18}F-FDG to evaluate clinical response in melanoma and, more generally, argue for further studies to explore the use of PET tracers that target apoptotic pathway activation or cell death.

Key Words: arginine deiminase; melanoma; ^{18}F-FDG; PI3K

J Nucl Med 2012; 53:281–286
DOI: 10.2967/jnumed.111.092973

Nutrient depletion therapy with arginine deiminase (ADI) has shown some promise in treating metastatic melanoma and hepatocellular carcinoma, in addition to preclinical models of renal, prostate, and pancreatic cancers (*1–5*). Sensitivity is believed to be associated with the deficient expression of argininosuccinate synthetase (ASS), a rate-limiting enzyme in the biosynthesis of L-arginine (*6*). Despite encouraging preclinical studies showing acute sensitivity to ADI, the clinical data for metastatic melanoma has been mixed—approximately 25% of patients respond to ADI treatment (*2*). It is, to date, unclear why only a subset of patients responds, and it is currently not possible to make projections about how a patient population will stratify.

Akin to the manner in which ^{18}F-FDG uptake has simplified the interpretation of response in gastrointestinal stromal tumors after imatinib therapy (*7*), a molecular imaging tool could, in principle, more clearly define (or predict) tumor response to ADI therapy. Indeed, PET/CT with ^{18}F-FDG has recently been adopted alongside other criteria (e.g., Response Evaluation Criteria in Solid Tumors) to guide the clinical assessment of ADI therapy (*8*). However, there is so far no report demonstrating that ^{18}F-FDG can document tumor response to ADI therapy. Consequently, the purpose of this study was to more systematically examine ^{18}F-FDG responses in preclinical models demonstrated to be sensitive to ADI therapy.

MATERIALS AND METHODS

Materials

The melanoma cell lines SK-MEL 10 and SK-MEL 28 were obtained from Memorial Sloan-Kettering Cancer Center (MSKCC) and maintained in glucose-containing RPMI and Dulbecco modified Eagle medium, respectively, supplemented with 10% fetal calf serum, L-glutamine, and penicillin–streptomycin (100 μg/mL) at 37°C and 5% CO_2. Transcript levels were determined with the following primers (IDT): ASS (forward: 5′-CCTAGCCCTGAGTGTGAATTTGTCC-3′; reverse: 5′-AGTGACCTTGCTCTGGAGACGATGA-3′) and p53 (forward: 5′-TACTCCCCTGCCCTCAACAAG-3′; reverse: 5′-CTCAGGCGGCTCATAGGG-3′). Commercial primers were used

Received May 10, 2011; revision accepted Sep. 29, 2011.
For correspondence or reprints contact: Lars Stelter, Department of Radiology and Nuclear Medicine, Charité University Medicine Berlin, Campus Virchow-Klinikum, Augustenburger Platz 1, 13353 Berlin, Germany.
E-mail: lars.stelter@charite.de
Published online Jan. 6, 2012.

to determine phosphatase and tensin homolog (PTEN) and glucose transporter 1 (GLUT1) expression levels (Superarray Biosciences). ADI-PEG 20 (DesigneRx Pharmaceuticals Inc., a subsidiary of Polaris Group) and MG-132 (Calbiotech) were obtained and used without further purification. For immunoblot analysis of protein expression levels, α-ASS (BD Biosciences), α-caspase 3 (Cell Signaling Technologies), α-poly (ADP-ribose) polymerase (PARP) (Promega) or α-actin (AC-15, GeneTex), α-PTEN (Santa Cruz Biotechnology), α-phosphoAkt (S473, Cell Signaling Technologies), α-Akt (Cell Signaling Technologies), α-GLUT1 (Abcam), and α-mouse and α-rabbit IgG-horseradish peroxidase secondary antibodies (Santa Cruz Biotechnology) were used according to manufacturer's instructions. Statistical analysis of all data (Student *t* test) was performed with Prism 5.0 (GraphPad) and Microsoft Excel 2008 for Mac (version 12.0). A *P* value of less than 0.05 was regarded as significant. Error bars represent SEM.

In Vitro Proliferation Studies

SK-Mel 10 and SK-MEL 28 cells (5×10^3) were plated in 96-well plates and assayed in triplicate. Cells were treated with vehicle or ADI-PEG 20 (4.3 mU/mL) daily for 1 wk or once a week for 8 wk. The dose was backcalculated from the optimum biologic dose (160 U/m^2) for melanoma patients (*2*) with the following equation: 160 U/m^2 = approximately 300 U/1.86 m^2 (body surface area of a 70-kg/177-cm human [70 kg = 70,000 cm^3]), resulting in 300 U/70,000 cm^3 = 4.3 mU/cm^3 (~0.48 μg of ADI-PEG 20 per cubic centimeter). After the indicated period, proliferation was assessed with the WST-1 proliferation kit (Roche Diagnostics GmbH) according to manufacturer's instructions, and absorption was read in a microplate reader (Safire; Tecan) at 450 nm (reference wavelength of 690 nm).

ADI Dosing Studies in Xenograft Models

All animal studies were conducted in accordance with the institutional guidelines established at MSKCC. Subcutaneous SK-MEL 28 xenografts were established by injecting 4×10^6 cells in Matrigel (BD Biosciences) in the shoulder region of 6- to 8-wk-old female nonobese diabetic–severe combined immune-deficient (SCID) mice (NOD.CB17-Prkdcscid/J; Jackson Laboratory). The mice were randomized into control (phosphate-buffered saline [PBS], $n = 3$) and ADI groups ($n = 5$). Seven days after inoculation (average tumor volume, ~500 mm^3), the mice received weekly intramuscular injections of ADI (160 U/m^2, ~17.8 mg/m^2) or PBS. Body weight, tumor volume (calculation: $2/3\ \pi \times [(\text{diameter } 1 + \text{diameter } 2)/2]^3$) were measured, and blood was withdrawn once a week over 8 wk.

Metabolite Analysis of Blood Samples

To determine the effect of ADI treatment in vivo, amino acid analysis of murine plasma samples was performed using high-performance liquid chromatography. L-Arginine and L-citrulline were resolved with a PCX 5200 postcolumn derivitization instrument (Pickering Laboratories) at 39°C reaction temperature and a fluorescence detector. All reagents, including the buffer and column, were used as suggested by Pickering Laboratories and as described previously (*1,2,9*).

Reverse-Transcription Polymerase Chain Reaction

To identify the ASS expression levels of our cell lines, reverse transcription polymerase chain-reaction was performed. RNA isolation was performed using the Ambion RiboPure Kit (Applied Biosystems Inc.) according to the manufacturer's protocol. Complementary DNA was prepared using M-MLV reverse transcriptase (Invitrogen) according to the manufacturer's instructions.

Immunoblot Analysis of Protein Expression Levels

SK-MEL 10 and SK-MEL 28 cells were harvested for protein analysis using M-PER (Thermo Scientific) supplemented with protease and phosphatase inhibitors (Calbiochem). Protein concentration was determined with a Bradford protein assay (Bio Rad) and bovine serum albumin standards. Samples were prepared in lithium dodecyl sulfate sample buffer (Invitrogen), and cell lysates (25–75 μg/lane) were resolved by gel electrophoresis. Lysate samples were transferred, blocked (SuperBlock Blocking Buffer; Thermo Scientific), and probed for expression with primary antibodies for 12 h at 4°C. After incubation with the appropriate secondary antibody (1 h at room temperature), proteins were visualized with chemoluminescence (ECL, SuperSignal West Pico; Thermo Scientific).

Annexin V Detection

SK-MEL 28 cells were treated with ADI over a period of 7 d in 6-well plates as described. Annexin V and 4′,6-diamidino-2-phenylindole (DAPI) staining was used to differentiate apoptotic from dead cells per the manufacturer's recommended protocols (BD Biosciences). For fluorescence-activated cell sorting (FACS), cells were trypsinized, washed in ice-cold PBS, and placed in FACS tubes. After being washed in FACS buffer (PBS with 0.5% bovine serum albumin and 0.1% sodium azide), about 1×10^6 cells/mL were incubated for 30 min at 4°C with fluorescein isothiocyanate–labeled annexin V and DAPI in the dark and washed twice with FACS buffer. The stained cells were resuspended in FACS buffer and analyzed (annexin V–positive, annexin V–negative, DAPI-positive, and DAPI-negative) on a FACSCalibur LSR II flow cytometer (BD Biosciences) with CellQuest Pro, DiVA (BD Biosciences), and FlowJo software (TreeStar).

^{18}F-FDG Uptake In Vitro

SK-MEL 28 cells (2×10^6) were plated in culture flasks and assayed in triplicate. Cells were treated with vehicle or ADI-PEG 20 (4.3 mU/mL) daily for 2 wk, followed by an incubation period with 10 mL of culture medium containing 3.7 MBq (0.1 mCi) of ^{18}F-FDG. After 1 h of incubation, the cells were harvested and a liquid scintillation counter was used to assay the radioactivity in the medium and in the cell pellets. Percentage uptakes of ^{18}F-FDG in cells were determined using the following formula: (net counts in cell pellet)/(net counts in cell pellet + net counts in medium) × 100%. A sample of cells from each flask was withdrawn after harvest to determine the number of viable cells in each group. Finally, the activity measured in each cell sample was normalized to the number of viable cells.

PET of Xenograft Models

PET was performed also once a week before each treatment. Therefore, mice were kept fasting for 4 h and subsequently injected with about 11.1 MBq (0.3 mCi) of ^{18}F-FDG via a lateral tail vein. After 1 h of tracer uptake, in which the animals were kept anesthetized with 1%–2% isoflurane (Baxter Healthcare) and kept at an environmental temperature of 22°C–25°C, PET was performed on an R4 microPET (Concorde Microsystems Inc.), a dedicated 3-dimensional small-animal PET scanner. An energy window of 350–750 keV and a coincidence timing window of 6 ns were used, with a minimum of 20 million events, typically acquired over 5 min. The resulting list-mode data were sorted into 2-dimensional histograms by Fourier rebinning, and transverse images were reconstructed by filtered backprojection into a $128 \times 128 \times 63$ ($0.72 \times 0.72 \times 1.3$ mm) matrix. The reconstructed spatial resolution for ^{18}F is 2.2 mm in full width at half maximum at the center of the field of view to

3.2 mm in full width at half maximum offset 5 cm from the center of the field of view. The image data were corrected for nonuniformity of response of the small-animal PET, dead-time count losses, and physical decay to the time of injection, but no attenuation or scatter correction was applied. An empirically determined system calibration factor (i.e., MBq/cm^3/cps/voxel) for mice was used to convert voxel counting rates to activity concentrations, and the resulting image data were then normalized to the administered activity to determine by region-of-interest analysis the maximum percentage injected dose per gram of tumor corrected for radioactive decay to the time of injection in the tumors, using the ASIPro VM software (Concorde Microsystems Inc.). To further analyze the PET data, we also corrected the region-of-interest values to the partial-volume effect, applying an empirically determined equation (measured activity concentration $\times \{1 - e^{-0.80 \times (\text{source diameter} - 2.90)}\}$).

Immunohistochemistry

Immunohistochemistry was performed on sections of paraffin-embedded SK-MEL 28 xenografts after up to 7 wk of either ADI or PBS treatment. Briefly, sections were first deparaffinized in xylene and then rehydrated in a series of graded alcohols. As primary reagents, murine monoclonal antibody clone 195-21-1 to ASS and murine anti-PTEN monoclonal antibody clone 6H2.1 (Dako) were used. After an initial blocking step, primary antibodies were applied overnight at 5°C. Both a negative control (no primary antibody) and a positive control (liver for ASS, kidney for PTEN) were used. The primaries were detected with a biotinylated horse-antimouse secondary antibody (Vector Labs), followed by an avidin–biotin complex tertiary (ABC Elite; Vector Labs). Diaminobenzidine (Liquid DAB; Biogenex) served as a chromogen.

RESULTS

We first examined the sensitivity of 2 melanoma cell lines, SK-MEL 28 and SK-MEL 10, to ADI treatment in vitro. Consistent with the model of ADI potency, proliferation of SK-MEL 28 (ASS-negative; Supplemental Figs. 1A and 1B; supplemental materials are available online only at http://jnm.snmjournals.org) was greatly inhibited by ADI therapy, whereas SK-MEL 10 (ASS-positive, Supplemental Figs. 1A and 1B) was unaffected (Fig. 1A; 1 wk, daily dose study). We next examined the effects of ADI in SK-MEL 28 in vivo. ADI or vehicle (PBS) was administered once weekly for several weeks. We observed reductions of tumor volume among the ADI-treated group out to 4 wk (Fig. 1B), a time point at which durable reductions of serum L-arginine levels (Fig. 1C) and elevations in L-citrulline (the precursor of L-arginine within the urea cycle) levels (Supplemental Fig. 2) had been achieved. ASS expression in the xenografts remained unchanged and was not influenced by ADI (Supplemental Fig. 3). Collectively, these results suggested that SK-MEL 28 is a suitable model to study ADI-sensitive melanoma.

We next asked if ADI therapy could trigger acute or durable declines in tumor uptake of ^{18}F-FDG. To this end, subcutaneous SK-MEL 28 xenografts were established, and mice were imaged before initiating therapy. Mice were subsequently randomized and treated with vehicle or ADI, and animals were imaged with ^{18}F-FDG 1 time per week for several weeks. The results from the PET study showed visually obvious differences in tumor uptake of ^{18}F-FDG

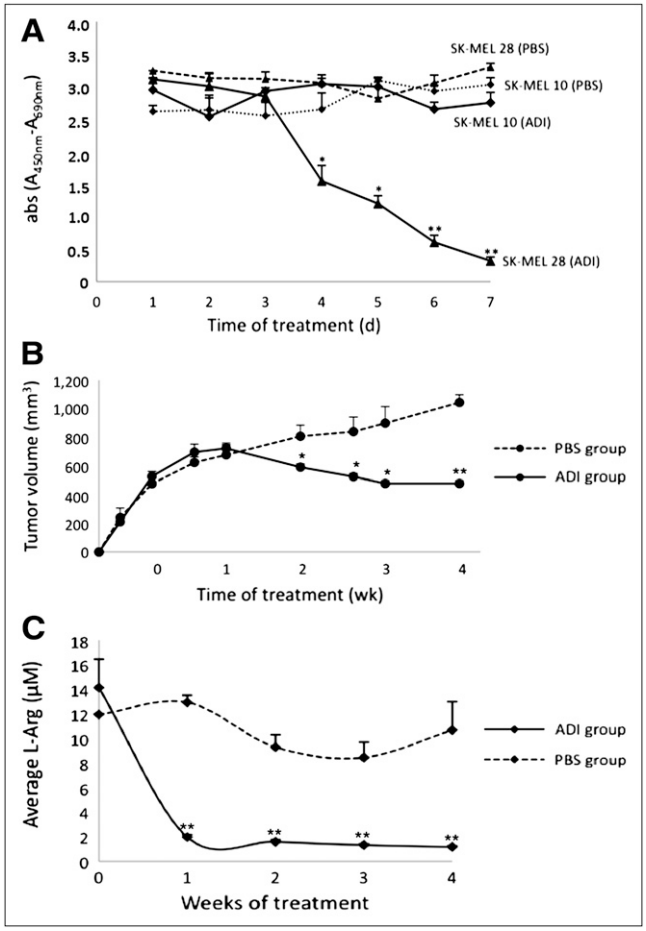

FIGURE 1. Profiling sensitivity of melanoma models to ADI. (A) SK-MEL 28 (ASS-negative) and SK-MEL 10 (ASS-positive) were treated with ADI (4.3 mU/mL) or vehicle (PBS) for 7 d (daily dose study), and proliferation was evaluated daily. Proliferation of SK-MEL 28 steadily declined out to 7 d with ADI treatment, whereas SK-MEL 10 was unaffected. (B) Subcutaneous SK-MEL 28 xenografts were established in female SCID mice, and animals were treated weekly with intramuscular injections of ADI (160 U/m^2) or vehicle (PBS). Tumor volume declined continuously from 1 to 4 wk of ADI treatment. Blood was drawn weekly (before next dosing) to confirm decrease in arginine levels (C) associated with effective therapeutic intervention. Bars represent SEM (*$P < 0.05$, **$P < 0.01$). abs = absorption; L-arg = L-arginine.

in the vehicle versus ADI-treated groups (Fig. 2A). However, quantitative analysis of the PET data showed that the differences were due to an increase in ^{18}F-FDG uptake in the vehicle group over time, rather than a decrease associated with ADI treatment (Fig. 2B). Indeed, tumor avidity for ^{18}F-FDG in the ADI-treated animals remained unchanged over time, despite clear regressions in tumor volume. This observation persisted with further refinements of the image analysis methodology (Supplemental Fig. 4).

This surprising result suggested to us that, despite its therapeutic benefit, ADI might affect an aspect of the biology that promotes ^{18}F-FDG uptake. A large body of literature has shown that activation of the PI3K/Akt signaling axis can result in elevated glycolysis, via posttranslational and transcriptional mechanisms (*10–12*). We therefore exam-

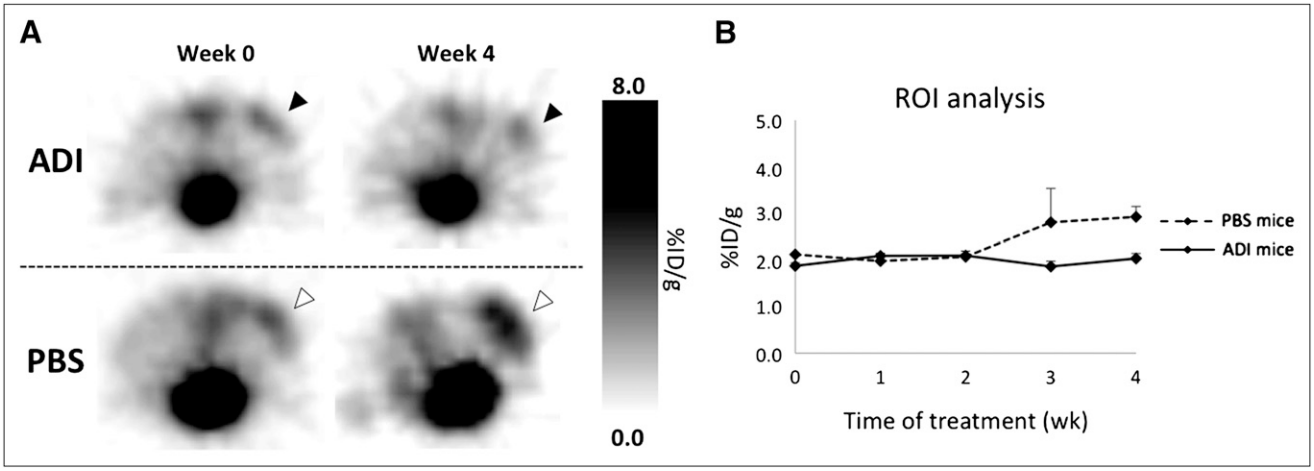

FIGURE 2. ^{18}F-FDG PET does not reveal early tumor response to ADI therapy in SK-MEL 28 xenografts. (A) Subcutaneous SK-MEL 28 xenografts were established in female SCID mice, and mice were imaged immediately before (week 0) ADI therapy (160 U/m^2) and once weekly for 4 wk. Representative PET images before onset of treatment and from end of the study are shown. Arrowheads indicate region of ^{18}F-FDG uptake associated with xenograft. (B) Region-of-interest analysis of intratumoral ^{18}F-FDG uptake did not show metabolic response in proportion to tumor volume reductions associated with ADI therapy (Fig. 1B). Bars represent SEM. %ID/g = percentage injected dose per gram; ROI = region of interest.

ined the expression of components of this pathway and found that ADI treatment rapidly downregulated PTEN expression in vitro (Fig. 3A). Moreover, pAkt levels were elevated (Fig. 3A), suggesting that PTEN loss promotes downstream signaling through the PI3K/Akt/mTOR signaling axis. Loss of PTEN was also observed in ADI-treated xenografts (Fig. 3B), likely accounting for the results from the ^{18}F-FDG study.

To better appreciate the functional consequences of ADI-triggered PTEN loss, we measured the expression levels of GLUT1 and glucose transporter 4 after ADI treatment and found that transcript and protein levels were elevated (Figs. 3A and 3C). ^{18}F-FDG uptake was also significantly elevated in ADI-treated SK-MEL 28 in vitro, consistent with the in vivo study (Fig. 4). Probing the mechanism by which ADI regulates PTEN, we found no change in PTEN message level associated with ADI treatment over 2 wk (Fig. 3C), suggesting that ADI may downregulate PTEN through a posttranslational mechanism. Consistent with this hypothesis, we observed that

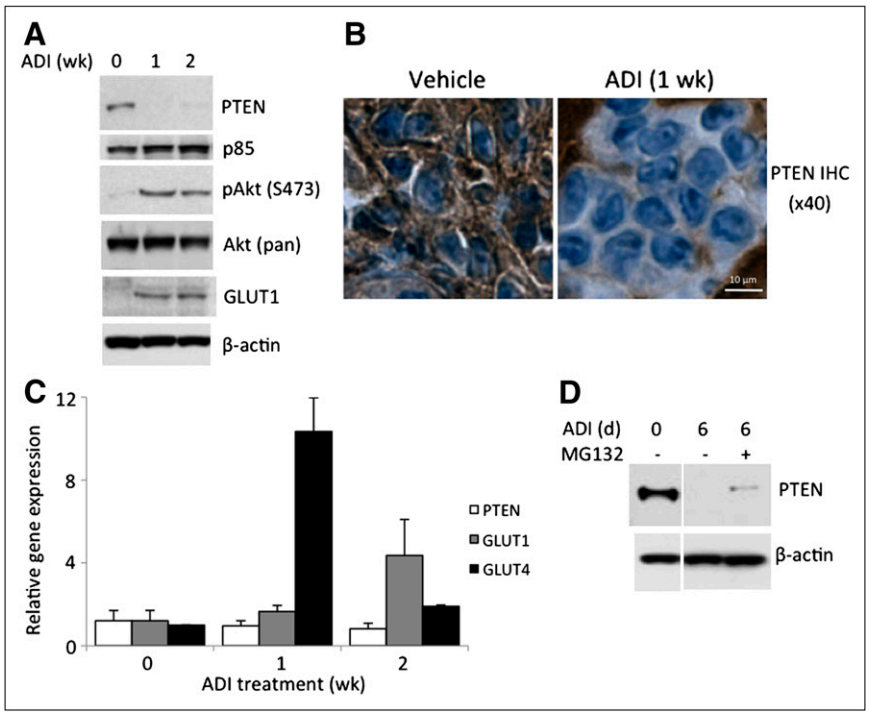

FIGURE 3. ADI treatment induces degradation of PTEN, resulting in downstream signaling events that promote ^{18}F-FDG uptake. (A) ADI treatment (4.3 mU/mL) acutely decreases PTEN expression and elevates PI3K (p85) and pAkt levels (S473). (B) Loss of PTEN was also observed in treated SK-MEL 28 xenografts (right) when compared with vehicle-treated tissue (left) by immunohistochemistry. (C) Alterations in PI3K/Akt signaling also increased expression of GLUT1 protein levels, in addition to GLUT1 and glucose transporter 4 transcript levels in vitro (see also part A of this figure), likely accounting for inability of ^{18}F-FDG to distinguish effects of ADI therapy. (D) To explore mechanism of PTEN loss, SK-MEL 28 cells were treated with ADI for 6 d, at which time proteasome inhibitor MG132 was added. PTEN levels were partially rescued by MG132 treatment, suggesting that ADI regulates PTEN levels via posttranslational mechanism. Consistent with this hypothesis, in vitro PTEN transcript levels were unaffected by ADI treatment over 2 wk (see also part C of this figure). Bars represent SEM. GLUT4 = glucose transporter 4; IHC = immunohistochemistry.

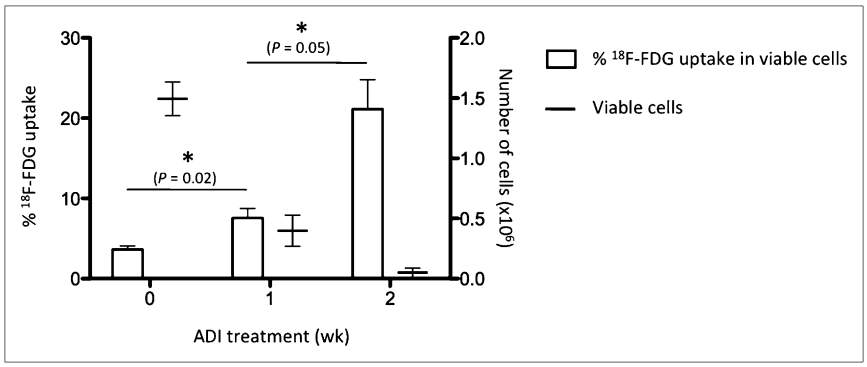

FIGURE 4. ^{18}F-FDG uptake in vitro is significantly increased among ADI exposure. After PTEN loss and upregulation of GLUT1, SK-MEL 28 clearly enhances intracellular ^{18}F-FDG uptake in weeks 1 and 2 of ADI treatment (bar graph), underlining inability of ^{18}F-FDG PET to monitor effects of ADI therapy. As cell viability significantly decreased on treatment (dash graph), cellular ^{18}F-FDG uptake was normalized to corresponding cell number and is expressed in percentage uptake. Bars represent SEM.

the proteasome inhibitor MG132 rescued PTEN expression in SK-MEL 28 treated with ADI (Fig. 3D). Collectively, these findings suggest that, for melanoma, the cross reactivity with the PI3K-signaling axis may preclude the use of ^{18}F-FDG for documenting clinical response to ADI treatment.

To advance alternative radiotracers better suited to documenting response to ADI therapy, we more thoroughly studied the mechanism of cell death associated with ADI treatment. Many radiotracers have been developed to detect tumor apoptosis; consequently, we probed for evidence of apoptosis by FACS analysis in SK-MEL 28 after ADI treatment. Clear evidence of apoptotic cell death was observed, as more than 90% of cells showed combined staining for annexin V and DAPI 7 d after treatment (Fig. 5A; Supplemental Fig. 5). SK-MEL 10 showed minimal staining at this time point, confirming the fidelity of the assay (Supplemental Fig. 6). We next probed for the specific pathway invoked to initiate apoptosis by immunoblot. We observed early and sustained PARP cleavage in SK-MEL 28 over a treatment period of 7 d (daily dose study) and no evidence of cleaved PARP in the untreated control (Fig. 5B). Conversely, caspase-3 did not seem to be involved in ADI-mediated cell death, because we observed no evidence of cleaved caspase over a similar dosing course of ADI (Fig. 5B).

DISCUSSION

Although the antitumor effects associated with nutrient deprivation have been known for several years, there has been little progress in the development of noninvasive markers to project response (*13–16*). In this study, we have shown that ^{18}F-FDG, a radiotracer currently involved in clinical trials to evaluate ADI, may not accurately reflect effective therapeutic intervention with ADI, because of an unexpected proglycolytic response associated with PTEN degradation and upregulation of PI3K signaling. These results underscore the importance of developing a thorough mechanistic characterization of drug pharmacology to select an appropriate diagnostic test.

Our findings raise the possibility that loss of PTEN may also attenuate the antiproliferative effects associated with ADI therapy in melanoma. Indeed, our preliminary work combining ADI and PI3K pathway–directed therapies shows enhancement of cell death beyond that conferred by single-agent therapy (data not shown). Because many patients

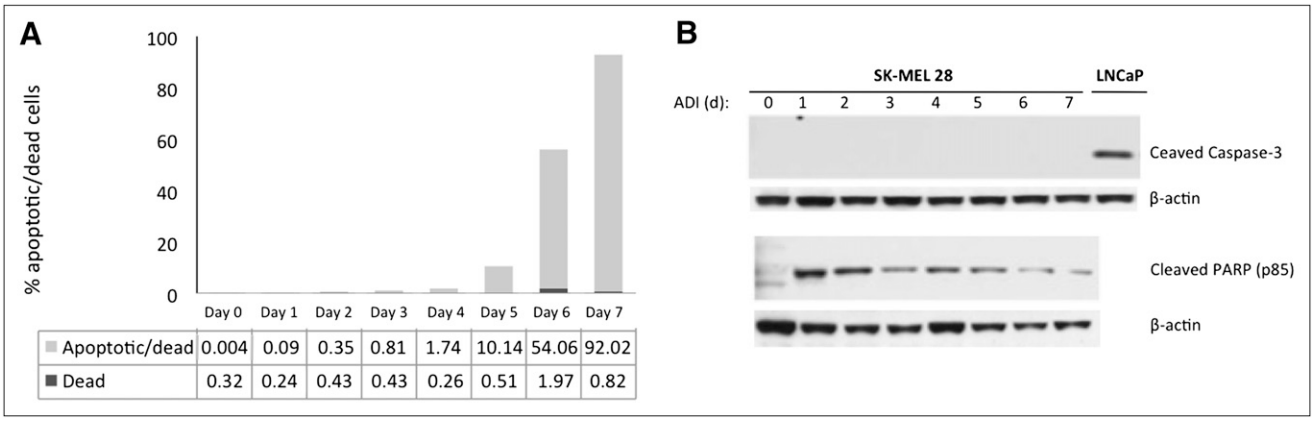

FIGURE 5. SK-MEL 28 undergoes caspase 3–independent apoptosis. (A) FACS analysis of ADI-treated SK-MEL 28 cells showed evidence of apoptotic cell death by day 7 (gray bars indicate annexin V–positive and DAPI-positive cells). Small percentage of dying cells did not show evidence of apoptosis (black bars indicate annexin V–negative and DAPI-positive cells). (B) Mechanism of apoptosis was investigated by immunoblotting, and ADI-triggered apoptosis in SK-MEL 28 appears to be caspase 3–independent, because no evidence of cleaved caspase 3 was detected over 7 d of treatment. Alternatively, ADI does induce PARP cleavage, suggesting its involvement in apoptotic cell death.

progress on ADI therapy despite compelling evidence of target inhibition (reduced serum levels of L-arginine levels) (*1,2,9*), the findings from this study may uncover a prosurvival mechanism operative in patients. Future studies are required to elaborate this point more clearly.

The mechanism by which ADI degrades PTEN is unclear. There are several reports that have characterized aspects of PTEN recycling via ubiquitination and proteasomal degradation, including the recent identification of NEDD4, an E3 ubiquitin ligase, as a key regulator of PTEN stability (*17–19*). Other reports have shown PTEN phosphorylation by the serine/threonine kinase CK2 (*20*), or the kinase PLK3 regulate ubiquitinylation of PTEN (*21*). We have found no evidence in the literature linking L-arginine biosynthesis to any of these events, and this remains a frontier in the community's understanding of PTEN regulation.

CONCLUSION

We demonstrate that caution should be approached in the use of ^{18}F-FDG for the evaluation of ADI therapy. Alternatively, the molecular features of cell death reported herein seem to suggest that a radiotracer measuring proliferation (e.g., 3′-deoxy-3′-^{18}F-fluorothymidine) or apoptotic cell death (e.g., ^{124}I-annexin V) could more accurately report the antitumor activity associated with nutrient depletion, and we are actively exploring these possibilities.

DISCLOSURE STATEMENT

The costs of publication of this article were defrayed in part by the payment of page charges. Therefore, and solely to indicate this fact, this article is hereby marked "advertisement" in accordance with 18 USC section 1734.

ACKNOWLEDGMENTS

We thank Dr. Marcus Kelly for informative discussions and Valerie Longo and Ramon Chua for technical assistance. We also thank Dr. Il-Kang Na for obtaining the FACS analysis and the staff of the Radiochemistry/Cyclotron Core at MSKCC. Technical services provided by the MSKCC Small-Animal Imaging Core Facility were supported in part by NIH grants R24 CA83084 and P30 CA08748. Technical services provided by the MSKCC Small-Animal Imaging Core Facility were supported in part by the NIH (R24 CA83084 and P30 CA08748). Portions of the study were also supported by the Deutsche Forschungsgemeinschaft (Ste 1837/1-1), a training grant in Molecular Imaging from the National Cancer Institute (2R25-CA096945), the Brain Tumor Center at MSKCC, and the Ludwig Center for Cancer Immunotherapy at MSKCC and the National Cancer Institute (P50-CA86483). John S. Bomalaski is the executive vice-president of Polaris Group, the company that manufactures and holds patents related to ADI-PEG 20. This article makes no claims about the efficacy of ADI-PEG 20. No other potential conflict of interest relevant to this article was reported.

REFERENCES

1. Izzo F, Marra P, Beneduce G, et al. Pegylated arginine deiminase treatment of patients with unresectable hepatocellular carcinoma: results from phase I/II studies. *J Clin Oncol.* 2004;22:1815–1822.
2. Ascierto PA, Scala S, Castello G, et al. Pegylated arginine deiminase treatment of patients with metastatic melanoma: results from phase I and II studies. *J Clin Oncol.* 2005;23:7660–7668.
3. Yoon CY, Shim YJ, Kim EH, et al. Renal cell carcinoma does not express argininosuccinate synthetase and is highly sensitive to arginine deprivation via arginine deiminase. *Int J Cancer.* 2007;120:897–905.
4. Kim RH, Coates JM, Bowles TL, et al. Arginine deiminase as a novel therapy for prostate cancer induces autophagy and caspase-independent apoptosis. *Cancer Res.* 2009;69:700–708.
5. Bowles TL, Kim R, Galante J, et al. Pancreatic cancer cell lines deficient in argininosuccinate synthetase are sensitive to arginine deprivation by arginine deiminase. *Int J Cancer.* 2008;123:1950–1955.
6. Dillon BJ, Prieto VG, Curley SA, et al. Incidence and distribution of argininosuccinate synthetase deficiency in human cancers. *Cancer.* 2004;100:826–833.
7. Choi H, Charnsangavej C, Faria SC, et al. Correlation of computed tomography and positron emission tomography in patients with metastatic gastrointestinal stromal tumor treated at a single institution with imatinib mesylate: proposal of new computed tomography response criteria. *J Clin Oncol.* 2007;25:1753–1759.
8. Eisenhauer EA, Therasse P, Bogaerts J, et al. New response evaluation criteria in solid tumours: revised RECIST guideline (version 1.1). *Eur J Cancer.* 2009;45:228–247.
9. Glazer ES, Piccirillo M, Albino V, et al. Phase II study of pegylated arginine deiminase for nonresectable and metastatic hepatocellular carcinoma. *J Clin Oncol.* 2010;28:2220–2226.
10. Rosivatz E. Inhibiting PTEN. *Biochem Soc Trans.* 2007;35:257–259.
11. Nakashima N, Sharma PM, Imamura T, Bookstein R, Olefsky JM. The tumor suppressor PTEN negatively regulates insulin signaling in 3T3-L1 adipocytes. *J Biol Chem.* 2000;275:12889–12895.
12. Rodríguez-Escudero I, Roelants FM, Thorner J, Nombela C, Molina M, Cid VJ. Reconstitution of the mammalian PI3K/PTEN/Akt pathway in yeast. *Biochem J.* 2005;390:613–623.
13. Gilroy E. The influence of arginine upon the growth rate of a transplantable tumour in the mouse. *Biochem J.* 1930;24:589–595.
14. Gonzales GG, Byus CV. Effect of dietary arginine restriction upon ornithine and polyamine metabolism during two-stage epidermal carcinogenesis in the mouse. *Cancer Res.* 1991;51:2932–2939.
15. Bach SJ, Swaine D. The effect of arginase on the retardation of tumor growth. *Br J Cancer.* 1965;19:379–384.
16. Lam TL, Wong GKY, Chong HC, et al. Recombinant human arginase inhibits proliferation of human hepatocellular carcinoma by inducing cell cycle arrest. *Cancer Lett.* 2009;277:91–100.
17. Ming M, He YY. PTEN: New insights into its regulation and function in skin cancer. *J Invest Dermatol.* 2009;129:2109–2112.
18. Wang X, Trotman LC, Koppie T, et al. NEDD4-1 is a proto-oncogenic ubiquitin ligase for PTEN. *Cell.* 2007;128:129–139.
19. Wang X, Shi Y, Wang J, Huang G, Jiang X. Crucial role of the C-terminus of PTEN in antagonizing NEDD4-1-mediated PTEN ubiquitination and degradation. *Biochem J.* 2008;414:221–229.
20. Torres J, Pulido R. The tumor suppressor PTEN is phosphorypated by the protein kinase CK2 at its C terminus. Implications for PTEN stability to proteasome-mediated degradation. *J Biol Chem.* 2001;276:993–998.
21. Xu D, Yao Y, Jiang X, Lu L, Dai W. Regulation of PTEN stability and activity by Plk3. *J Biol Chem.* 2010;285:39935–39942.